Unveiling the microscopic nature of correlated organic conductors: The case of κ-$(ET)_2Cu[N(CN)_2]Br_xCl_{1-x}$

Johannes Ferber, Kateryna Foyevtsova, Harald O. Jeschke,* and Roser Valentí†
Institut für Theoretische Physik, Goethe-Universität Frankfurt, Max-von-Laue-Strasse 1, 60438 Frankfurt/Main, Germany
(Received 5 February 2014; published 8 May 2014)

A few organic conductors show a diversity of exciting properties like Mott insulating behavior, spin liquid, antiferromagnetism, bad metal, or unconventional superconductivity controlled by small changes in temperature, pressure, or chemical substitution. While such a behavior can be technologically relevant for functional switches, a full understanding of its microscopic origin is still lacking and poses a challenge in condensed matter physics since these phases may be a manifestation of electronic correlation. Here we determine from first principles the microscopic nature of the electronic phases in the family of organic systems κ-$(ET)_2Cu[N(CN)_2]Br_xCl_{1-x}$ by a combination of density functional theory calculations and the dynamical mean field theory approach in a form adapted for organic systems. By computing spectral and optical properties we are able to disentangle the origin of the various optical transitions in these materials and prove that correlations are responsible for relevant features. Remarkably, while some transitions are inherently affected by correlations, others are completely uncorrelated. We discuss the consequences of our findings for the phase diagram in these materials.

DOI: 10.1103/PhysRevB.89.205106 PACS number(s): 71.27.+a, 74.20.Pq, 74.70.Kn, 71.15.Ap

One of the most intensively debated open questions in condensed matter physics is the emergence of exotic phases like spin liquid or unconventional superconductivity in a Mott insulator upon changes in temperature, doping, or pressure. In particular, an increasingly prominent class of materials with an abundance of correlated phases are the κ-based organic charge transfer salts containing the molecules bis-(ethylenedithio)tetrathiafulvalene (BEDT-TTF, or shorter ET) [1,2]. In these κ-$(ET)_2X$ salts, electron donors (ET) and electron acceptors (X) form alternating layers, with pairs of ET molecules forming dimers $(ET)_2$ arranged in a triangular lattice (see Fig. 1). For monovalent anions X one electron is transferred from each dimer $(ET)_2$ to each anion formula unit so that the system is half-filled. Band structure calculations [3,4] therefore predict the dimer layers to be metallic. However, the experimentally observed ground state depends on the choice of the anion: Even for the example of the isostructural compounds κ-$(ET)_2Cu[N(CN)_2]Cl$ (in short κ-Cl) and κ-$(ET)_2Cu[N(CN)_2]Br$ (κ-Br), the ground state can be as different as a Mott insulator for κ-Cl and a Fermi liquid for κ-Br at low temperatures and ambient pressure [5]. κ-Cl can be driven through the insulator-to-metal transition (MIT) by the gradual substitution of Cl for isovalent Br. In the high-temperature regime κ-Cl is a semiconductor with a gap of $E_g = 800$ K [6], while κ-Br shows "bad metal" behavior with strong scattering preventing coherent transport and suppressing the Drude peak.

The fact that small chemical modifications lead to qualitative changes in behavior together with the possible importance of electronic correlations in these materials make it clear that a realistic description requires both (i) details of the band structure as well as (ii) a proper treatment of electronic correlations. However, many-body studies of the κ-$(ET)_2X$ salts have so far been limited to minimal model calculations [7–9] of the Hubbard or extended Hubbard Hamiltonian on an anisotropic triangular lattice [10]. In this work we go beyond model calculations and present a combination of *ab initio* density functional theory calculations in the full potential linearized augmented plane wave (FLAPW) framework [11] combined with DMFT [12] (local density approximation plus dynamical mean field theory, LDA + DMFT). Also, in order to perform these calculations for organic systems, we propose a generalization of previously introduced Wannier projectors [12].

We show that this first-principles approach provides insight into the contributions to the optical conductivity at an unprecedented level; (i) we find that interdimer and intradimer transitions are responsible for two principal features resolved in optical conductivity measurements at low temperatures, (ii) we unambiguously identify the interdimer feature to be related to correlations, and (iii) we are able to unveil the origin of the anisotropic conductivity (light polarization dependent). These calculations go beyond previous conjectures based on phenomenological and minimal model assumptions [13,14].

While recent LDA + DMFT calculations on organic molecular crystals employed Wannier functions with a single atomic character [15], the electronic structure of organic charge transfer salts requires the construction of localized Wannier functions from the entire highest occupied molecular orbital (HOMO). A fast and stable method to obtain Wannier functions consists in projecting Bloch states onto pure atomic orbitals with subsequent orthonormalization [12,16,17]. In its standard form, though, this method is not designed for molecular orbitals. In this work we propose a scheme to construct molecular Wannier functions using atomic orbitals as a starting point. The key element of this scheme is the diagonalization of the occupation matrix written in the basis of atomic orbitals within the subspace of the correlated bands (see Appendix A). The real space representation of the resulting dimer HOMO Wannier function of κ-Cl (based on the crystal structure reported in Ref. [18] with space group

*jeschke@itp.uni-frankfurt.de
†valenti@itp.uni-frankfurt.de

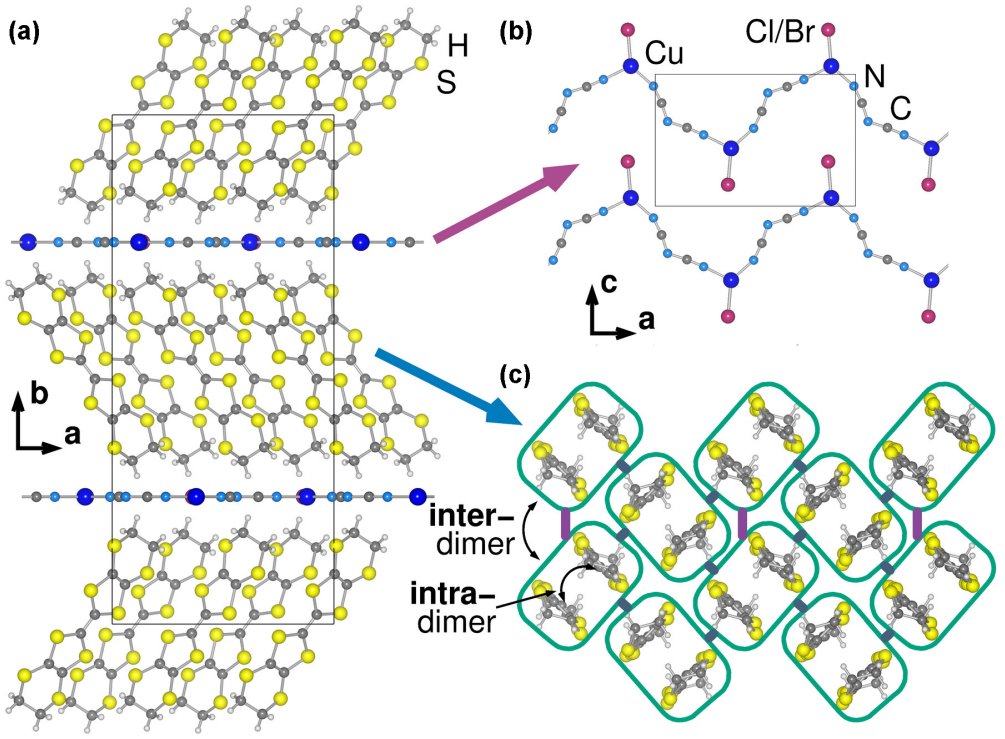

FIG. 1. (Color online) (a) Structure of κ-$(ET)_2Cu[N(CN)_2]Cl/Br$ seen in the ab plane. (b) and (c) Separate anion and cation layers projected in the ac plane.

$Pnma$) is shown in Fig. 2. Once the Wannier functions are obtained out of the LDA cycle, we employ the hybridization expansion continuous-time quantum Monte Carlo method [19] as implemented in the ALPS code [20,21] in order to solve the impurity problem in the DMFT cycle. We used 2×10^7 Monte Carlo sweeps throughout our calculations at an inverse temperature $\beta = 40$ eV^{-1}, corresponding to room temperature $T = 300$ K. Since the quantum Monte Carlo algorithm operates on the imaginary frequency axis, the calculation of dynamical quantities like spectral functions and optical conductivity requires analytic continuation to the real axis. We performed stochastic analytic continuation [22] on the self-energy for obtaining the spectral functions and directly on the optical conductivity $\sigma(i\nu)$ for the calculation of optical properties (see Appendix B).

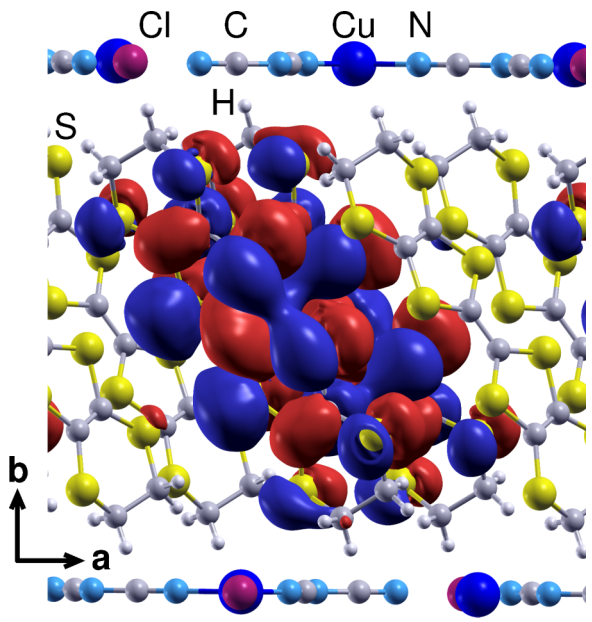

FIG. 2. (Color online) Structure of κ-$(ET)_2Cu[N(CN)_2]Cl$ seen in the ab plane with a Wannier function corresponding to the bands crossing the Fermi level.

In Figs. 3(a) and 3(b) we show the LDA + DMFT calculated band structure [23] of κ-$(ET)_2Cu[N(CN)_2]Br_xCl_{1-x}$ in the form of the momentum-resolved spectral function for Hubbard $U = 0.6$ eV [Fig. 3(b)] along with the LDA band energies [Fig. 3(a)]. The LDA calculations were done for the stoichiometric κ-Cl and κ-Br. We find only small changes of the LDA band structure [3] at E_F between both systems. The choice of $U = 0.6$ eV in the LDA + DMFT calculations is guided by two estimates: $U = 0.85$ eV obtained for a similar but arguably more strongly correlated compound κ-$(ET)_2Cu_2(CN)_3$ from constrained random phase approximation [4], and $U \approx 0.27$ eV extracted from optical conductivity measurements [13] and model considerations [9]. The LDA + DMFT bands [Fig. 3(b)] show a strong renormalization at $E_F = 0$ with respect to the LDA bands [Fig. 3(a)]. These bands originate from the interdimer hopping [see Fig. 1(c)], in particular hopping between dimers on the same layer; the interlayer hopping is very small, so that the four bands are composed of two almost degenerate pairs of bands. The correlation in band space acts almost exclusively on these bands, splitting them into renormalized excitations of (mass-enhanced) quasiparticles (blue-scale color map at $E_F = 0$) and a spectral weight transfer to an upper and lower Hubbard band which manifests itself as blurry background

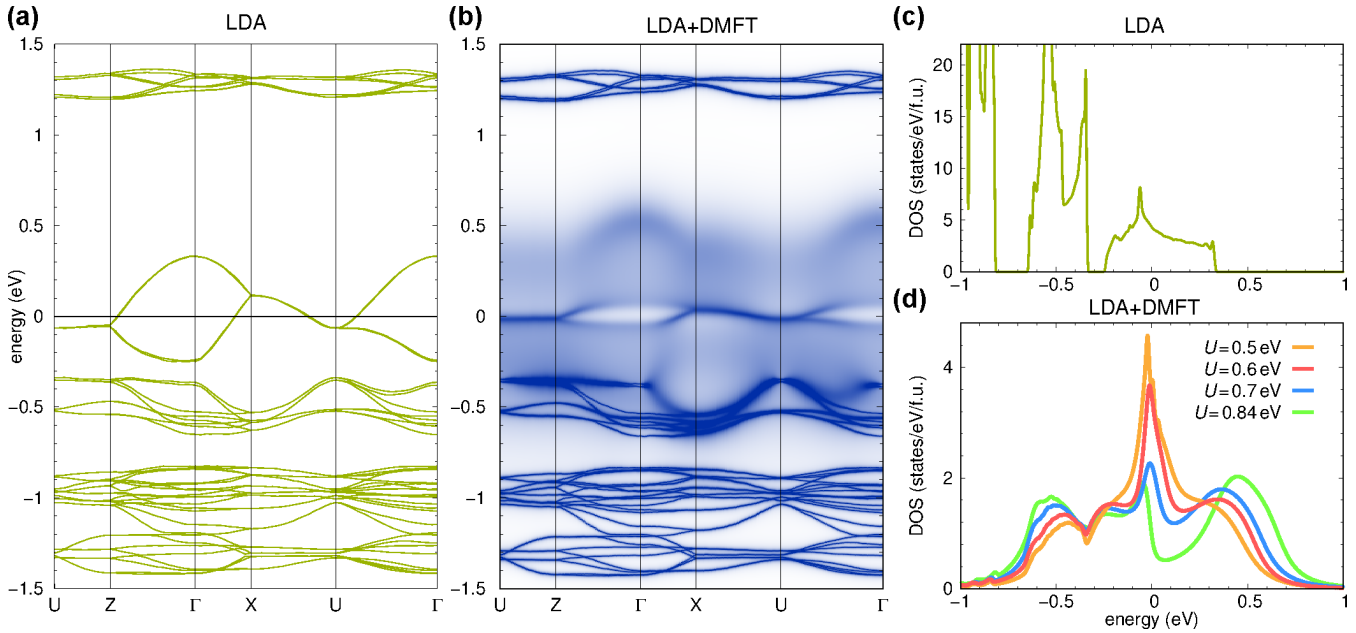

FIG. 3. (Color online) (a) LDA band structure of κ-$(ET)_2Cu[N(CN)_2]Cl$. (b) LDA + DMFT momentum-resolved spectral function for $U = 0.6$ eV. Note that the LDA + DMFT results are not sharp since the spectral function $A(k,\omega)$ is not a δ function. (c) LDA density of states, and (d) LDA + DMFT DOS (**k** integrated spectral function, for the projected manifold) for different values of the interaction strength U.

around -0.5 and 0.5 eV, respectively. On the other hand, the charge transfer between the ET molecules within a dimer [intradimer, see Fig. 1(c)] induces the splitting between the bands into bonding (around -0.4 eV) and antibonding bands (around the Fermi level). This splitting is less affected by correlations as can be observed by comparing Figs. 3(a) and 3(b).

Next, we investigate the optical properties of κ-$(ET)_2Cu[N(CN)_2]Br_xCl_{1-x}$ first with the light polarization $\mathbf{E} \parallel \mathbf{c}$ along the linear chains in the triangular lattice as measured experimentally [13,14]. At room temperature, the authors of Ref. [13] observed a broad midinfrared absorption peak between 1600 and 4200 cm^{-1}, in agreement with previous optical studies on κ-Cl and κ-Br (see Ref. [13] and references therein). At low temperature, a Drude peak evolves for the compounds with high Br concentration which marks the onset of metallicity at $x \approx 0.7$, whereas no Drude peak is visible for lower Br content indicating an insulating state without coherent quasiparticles. Importantly, at low temperatures ($T = 90$ K and below) the broad midinfrared peak (polarization $\mathbf{E} \parallel \mathbf{c}$) splits into two peaks in the pure Cl and low Br concentration compounds, which can be fitted by two Lorentzians at $\approx$2200 and 3200 cm^{-1}; for high Br content this splitting is very weak but it is still present. From this doping dependence, it was suggested [13] that the first peak is a correlation-induced feature due to electron transitions between the lower and upper Hubbard bands, while the second peak was assigned to the intradimer charge transfer (see Fig. 8 of Ref. [13]). In contrast, for polarization $\mathbf{E} \parallel \mathbf{a}$ the broad midinfrared peak does not show any splitting at low temperatures. This anisotropic behavior of the optical conductivity has remained unresolved up to now.

The method introduced in this work allows us to investigate the microscopic origin of the observed spectra. As the energy window of our LDA + DMFT calculation contains both the correlated manifold at the Fermi energy as well as uncorrelated bands away from E_F, all transitions can be inspected on equal footing. Our calculations are at $T = 300$ K (continuous-time QMC) and capture the effects of correlation contained in the $T = 300$ K data and observed as pronounced features in measurements below room temperature. We denote the transitions occurring at the Fermi level between (i) Hubbard bands and (ii) Hubbard bands and quasiparticle peak (if present) as *intra*band contributions (i.e., *interdimer* transitions) to the optical conductivity. All other transitions are termed *interband* transitions; among others, these contain transitions related to the *intradimer* charge transfer.

In Figs. 4(a)–4(c) we show the LDA and LDA + DMFT ($U = 0.6$ eV) calculated optical conductivity for polarization $\mathbf{E} \parallel \mathbf{c}$ and $\mathbf{E} \parallel \mathbf{a}$. We would like to note that while the LDA results change minimally between κ-Cl and κ-Br, they are extremely sensitive to the effects of correlation (U) as can be observed in the density of states [Figs. 3(c) and 3(d)] and in the optical conductivity [Fig. 4(d)]. For $U > 0.84$ eV a gap opens and the Drude peak disappears. This corresponds to the κ-Cl system although with a somewhat overestimated U value (this is a well-known limitation of single-site DMFT in low dimensions [24,25]). Smaller U values correspond to the conductivity behavior of κ-$(ET)_2Cu[N(CN)_2]Br_xCl_{1-x}$ at larger values of x. For $U = 0.6$ eV we observe a remnant of the Drude peak as it is the case in κ-$(ET)_2Cu[N(CN)_2]Br_xCl_{1-x}$ at moderate x.

For $\mathbf{E} \parallel \mathbf{c}$ the calculated LDA + DMFT total optical conductivity [Fig. 4(b)] features one dominant low-frequency peak at approximately 3450 cm^{-1}, i.e., close to the experimental peak position (we do not consider vibronic modes) [13]. The position of this peak is roughly centered at the same position as in the LDA results [Fig. 4(a)], but it is strongly enhanced in

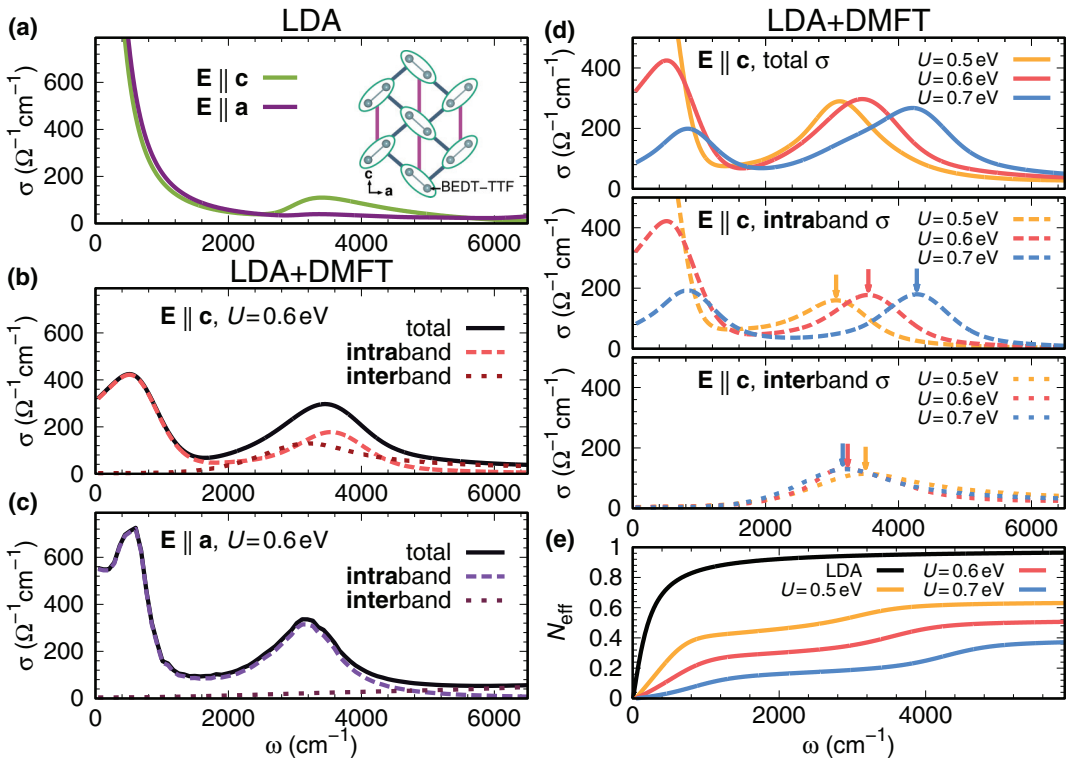

FIG. 4. (Color online) (a) Calculated LDA optical conductivity for two directions of the light polarization. (b) and (c) LDA + DMFT optical conductivity for $U = 0.6$ eV for electrical field along (a) and (c), respectively. (d) LDA + DMFT optical conductivity for different values of the interaction strength U. The arrows show the position of maxima for the intraband (middle panel) and the interband (lower panel) contributions. (e) Optical conductivity sum rule for LDA and LDA + DMFT at different U values.

spectral weight, in accordance with experiment [13]. While our calculations are at room temperature, they already capture the effects of correlation resolved in measurements at low T. We can decompose our data into intra- and interband contributions. $\sigma_{\text{interband}}$ contains contributions of transitions between almost uncorrelated bands and roughly coincides with the LDA results in position and spectral weight. This contribution shows a peak at $\omega \approx 3400$ cm^{-1} that corresponds to *intradimer* transitions [Fig. 4(b) dotted line]. In contrast, the intraband contribution $\sigma_{\text{intraband}}$ is centered at $\omega \approx 3550$ cm^{-1} $\approx 0.75\,U$ and it corresponds to the intraband Hubbard transitions [*interdimer* contribution, Fig. 4(b) dashed line]. Once thermal fluctuations are suppressed by lowering temperature, the two low frequency contributions (3400 and 3550 cm^{-1})—that come naturally out of our calculations—are experimentally observed as two distinguishable peaks, a "dimer" peak and a "Hubbard" peak, respectively [13].

In order to analyze the nature of the two low-frequency intraband and interband absorption peaks, Fig. 4(d) shows their evolution with U. The intraband contribution (interdimer transitions) to the conductivity shifts in frequency proportional to U, with the peak position consistently corresponding to $\approx 0.75\,U$, while the interband absorption peak at low frequencies (intradimer transitions) is largely insensitive to U. This analysis demonstrates the correlated nature of $\sigma_{\text{intraband}}$ and uncorrelated nature of $\sigma_{\text{interband}}$.

Quantitatively, the suppression of the Drude peak as a function of U and the redistribution of the intraband spectral weight is presented in Fig. 4(e) where we plot the integrated spectral weight $\int_0^{\omega} \sigma_{\text{intraband}}(\omega')d\omega'$ representing the effective number of charge carriers N_{eff}. In this representation, the number of charge carriers in LDA by definition equals the number of conduction electrons, i.e., one, and all the weight is concentrated in the (infinitesimally narrow) coherent Drude peak which is only broadened by temperature. Upon inclusion of correlations, the kinetic energy of the electrons is diminished, which corresponds to a mass enhancement (in Fermi liquid theory) or a reduction of the number of effective charge carriers as we observe.

Summarizing the above analysis, we have shown from first principles that the two finite-frequency peaks resolved in the experimental optical conductivity for $\mathbf{E} \parallel \mathbf{c}$ of κ-$(ET)_2Cu[N(CN)_2]Br_xCl_{1-x}$ at low temperatures originate, respectively, from correlation-induced intraband (interdimer) contributions scaling with U, and interband (intradimer) transitions which are unaffected by correlations. The fact that DMFT overestimates the critical U of the triangular lattice in two dimensions forces us to describe these systems at $T = 300$ K with a somewhat high interaction strength of $U = 0.6$ eV.

We focus now on the optical conductivity $\mathbf{E} \parallel \mathbf{a}$. The LDA optical conductivity is completely featureless for $\omega \approx 3400$ cm^{-1} [Fig. 4(a)]. Inclusion of correlation effects [Fig. 4(c)] shows the appearance of a peak at this frequency. This peak is therefore only a consequence of transitions between the lower Hubbard band/quasiparticle peak and the upper Hubbard band (interdimer contribution) and at low temperatures no splitting of the peak is therefore to be expected,

as observed experimentally [13], in contrast to the $\mathbf{E} \parallel \mathbf{c}$ case. Finally, we would like to note that while calculations were performed at $T = 300$ K, important information was obtained for the features observed at lower temperatures. Accurate calculations of the optical conductivity at lower temperatures requires the use of alternative impurity solvers [29] and is beyond the scope of the present study.

In conclusion, we presented a LDA + DMFT study on the spectral and optical properties of the organic charge transfer salts κ-$(ET)_2Cu[N(CN)_2]Br_xCl_{1-x}$. Our results provide an *ab initio* based theoretical evidence for the double-natured origin of the infrared peak in the optical conductivity of this system for $\mathbf{E} \parallel \mathbf{c}$ as well as for the single-natured origin of the infrared peak for $\mathbf{E} \parallel \mathbf{a}$. We could identify intraband transitions within the correlated manifold and interband transitions due to charge transfer within an ET dimer. The proposed projection method for constructing non-atom-centered Wannier functions in the FLAPW framework is computationally efficient and can be applied to a great variety of correlated organic as well as inorganic systems with (quasi-)molecular orbitals. This opens the possibility of investigating correlation effects in complex organic systems from first principles.

We acknowledge useful discussions with M. Dressel. We gratefully acknowledge financial support from the Deutsche Forschungsgemeinschaft through TR49 and FOR1346 and the allotment of computer time by CSC-Frankfurt and LOEWE-CSC.

APPENDIX A: CONSTRUCTION OF MOLECULAR WANNIER FUNCTIONS

Our procedure of constructing molecular Wannier functions is an extension of the FLAPW-based method described in Ref. [12]. It assumes that a basic molecular unit is known and provides a linear combination of the orbitals of those atoms forming the given molecular unit.

From the Bloch functions $|\psi^{\sigma}_{\mathbf{k}\nu}\rangle$ of a well converged LDA ground state we calculate auxiliary projectors $\tilde{P}^{\alpha,\sigma}_{m\nu}$ for momentum vector $\mathbf{k}$ as

$$\tilde{P}^{\alpha,\sigma}_{m\nu}(\mathbf{k}) = \left\langle u^{\alpha,\sigma}_{l}(E_{1l}) Y^{l}_{m} \middle| \psi^{\sigma}_{\mathbf{k}\nu} \right\rangle. \tag{A1}$$

Here σ, ν, α, and m are the spin, band, atomic, and orbital indices, respectively; $u^{\alpha,\sigma}_{l}(E_{1l})$ are solutions of the Schrödinger equation within the muffin tin sphere α at linearization energy E_{1l}, and Y^{l}_{m} are spherical harmonics. We consider the occupation matrix in the basis of pure atomic orbitals $\{\alpha,m\}$ for the narrow energy window W' comprising correlated Bloch bands at $\mathbf{k} = 0$,

$$\mathcal{O}^{\alpha,\alpha'}_{m,m'}(\sigma) = \sum_{\nu \in W'} \tilde{P}^{\alpha,\sigma}_{m\nu}(0) \tilde{P}^{\alpha',\sigma *}_{m'\nu}(0). \tag{A2}$$

Note that only the atoms that form a specific molecule are involved. For κ-$(ET)_2Cu[N(CN)_2]Cl$, we employed the 60 C $2p$ and 48 S $3p$ atomic orbitals on a (BEDT-TTF) dimer and diagonalized the respective occupation matrix within the four-band manifold at the Fermi level. The eigenvectors of $\mathcal{O}^{\alpha,\alpha'}_{m,m'}(\sigma)$ that correspond to the largest eigenvalues define the weights with which the atomic orbitals $\{\alpha,m\}$ contribute to the molecular orbitals of interest. Often, only one molecular orbital is thus obtained, as in the case of κ-$(ET)_2Cu[N(CN)_2]Cl$. This molecular orbital (orbitals) will have the dominant weight in the states within the W' interval. For this to hold at all $\mathbf{k}$ vectors, in some cases care is needed to introduce due exponential Bloch factors for atoms located outside the reference unit cell.

If $U^{\alpha}_{m}(\sigma)$ is the eigenvector of the atomic orbital weights, then

$$\tilde{\mathcal{P}}^{\sigma}_{M\nu}(\mathbf{k}) = \sum_{\alpha,m} U^{\alpha}_{m}(\sigma) \tilde{P}^{\alpha,\sigma}_{m\nu}(\mathbf{k}) \tag{A3}$$

are molecular auxiliary projectors, with M being the molecular orbital index. $U^{\alpha}_{m}(\sigma)$ can be applied to all symmetry related molecules in the unit cell.

Finally, the projectors $\tilde{\mathcal{P}}^{\sigma}_{M\nu}(\mathbf{k})$ are orthonormalized within the DMFT energy window W, which can be much larger than W', using

$$P^{\sigma}_{M\nu}(\mathbf{k}) = \sum_{M'} \{[O(\mathbf{k},\sigma)]^{-1/2}\}_{M,M'} \tilde{\mathcal{P}}^{\sigma}_{M\nu}(\mathbf{k}), \tag{A4}$$

with

$$O_{M,M'}(\mathbf{k},\sigma) = \sum_{\nu \in W} \tilde{\mathcal{P}}^{\sigma}_{M\nu}(\mathbf{k}) \tilde{\mathcal{P}}^{\sigma *}_{M'\nu}(\mathbf{k}). \tag{A5}$$

The energy window W for κ-$(ET)_2Cu[N(CN)_2]Cl$ for was chosen to range from -1.4 to 1.5 eV with respect to the Fermi energy E_{F}, encompassing 44 bands in total.

APPENDIX B: OPTICAL CONDUCTIVITY

We calculate the optical conductivity in imaginary frequencies as

$$\sigma_{zz}(\tilde{\nu}_n) = \frac{e^2}{4\pi\epsilon_0 V \tilde{\nu}_n \beta} \sum_{\nu\nu'\nu''\nu''',\mathbf{k},\sigma} v^{\nu\nu'}_{z,\mathbf{k}} v^{\nu''\nu'''}_{z,\mathbf{k}} \times \sum_{\omega_n} G^{\nu'\nu''}_{\mathbf{k}}(i\omega_n + i\tilde{\nu}_n) G^{\nu'''\nu}_{\mathbf{k}}(i\omega_n), \tag{B1}$$

with V the volume of the unit cell, band indices $\{\nu\nu'\nu''\nu'''\}$, lattice Green's functions $G_{\mathbf{k}}(i\omega_n)$, and $\tilde{\nu}_n$ (ω_n) bosonic (fermionic) Matsubara frequencies. The Fermi velocity $v^{\nu\nu'}_{\alpha,\mathbf{k}}$ is given by the dipole matrix element,

$$v^{\nu\nu'}_{\alpha,\mathbf{k}} = \frac{1}{m} \langle \mathbf{k},\nu | p_{\alpha} | \mathbf{k},\nu' \rangle, \tag{B2}$$

with p_{α} the α component of the momentum operator. The Fermi velocities are taken from WIEN2k as calculated by the `optic` program.

In practice, the summation over momenta in Eq. (B1) is performed in the irreducible Brillouin zone only and therefore needs to be supplemented by a symmetrization procedure. For the optical conductivity, the symmetrization acts on the product of the momentum matrix elements $v^{pq}_{\alpha,\mathbf{k}} v^{st}_{\beta,\mathbf{k}}$.

Let O_i ($i = 1, \ldots, N_s$) denote the real-space symmetry operation matrices (as opposed to symmetrization matrices in orbital space). Then, in terms of $v^{pq}_{\alpha,i}$,

$$\begin{pmatrix} v^{pq}_{x,i} \\ v^{pq}_{y,i} \\ v^{pq}_{z,i} \end{pmatrix} = O_i \begin{pmatrix} v^{pq}_{x} \\ v^{pq}_{y} \\ v^{pq}_{z} \end{pmatrix}, \tag{B3}$$

the symmetrized products are given as

$$\left\{v_\alpha^{pq}\, v_\alpha^{st}\right\}^{\mathrm{symm}} = \frac{1}{N_s}\sum_i v_{\alpha,i}^{pq}\, v_{\alpha,i}^{st} \tag{B4}$$

and

$$\left\{v_\alpha^{pq}\, v_\beta^{st}\right\}^{\mathrm{symm}} = \frac{1}{N_s}\sum_i \begin{cases} v_{\alpha,i}^{pq}\, v_{\beta,i}^{st} & \text{if } \det(O_i) = 1 \\ \left(v_{\alpha,i}^{pq}\, v_{\beta,i}^{st}\right)^* & \text{if } \det(O_i) = -1 \end{cases} \tag{B5}$$

for different α and β. Note that unlike for one-particle quantities, the symmetrization cannot be performed after the **k** summation because of the complex conjugation in Eq. (B5).

APPENDIX C: ANALYTIC CONTINUATION

While we could have used the analytically continued self-energy also for the calculation of $\sigma(\omega)$ on the real axis, we chose to calculate $\sigma(i\nu)$ on the imaginary frequency axis and proceed with a subsequent analytic continuation for performance reasons: The summation over all elements of the four-index conductivity tensor along with the frequency convolution involved in the calculation of σ scales as $N_b^4 \cdot N_f^2$, where N_b is the number of bands ($N_b = 44$) and N_f is the number of frequencies. While in imaginary frequencies N_f can be of the order of 100 at the temperature we considered, an accurate determination on the real frequency axis would require $N_f \approx 1000$. Due to the large number of bands involved in our calculations, this would make the direct real-frequency calculation of σ rather expensive.

[1] K. Kanoda and R. Kato, Annu. Rev. Condens. Matter Phys. **2**, 167 (2011).
[2] B. J. Powell and R. H. McKenzie, Rep. Prog. Phys. **74**, 056501 (2011).
[3] H. C. Kandpal, I. Opahle, Y.-Z. Zhang, H. O. Jeschke, and R. Valentí, Phys. Rev. Lett. **103**, 067004 (2009).
[4] K. Nakamura, Y. Yoshimoto, T. Kosugi, R. Arita, and M. Imada, J. Phys. Soc. Jpn. **78**, 083710 (2009).
[5] Below 35 K, κ-$(ET)_2Cu[N(CN)_2]Cl$ develops a weak magnetic order [26, 27], whereas κ-$(ET)_2Cu[N(CN)_2]Br$ enters a superconducting state at $T_c = 12$ K [28]. We are not considering these very low temperature phases here.
[6] S. Yasin, M. Dumm, B. Salameh, P. Batail, C. Mézière, and M. Dressel, Eur. Phys. J. B **79**, 383 (2011).
[7] J. Merino and R. H. McKenzie, Phys. Rev. B **61**, 7996 (2000).
[8] O. Parcollet, G. Biroli, and G. Kotliar, Phys. Rev. Lett. **92**, 226402 (2004).
[9] J. Merino, M. Dumm, N. Drichko, M. Dressel, and R. H. McKenzie, Phys. Rev. Lett. **100**, 086404 (2008).
[10] B. J. Powell and R. H. McKenzie, J. Phys. Condens. Matter **18**, R827 (2006).
[11] P. Blaha, K. Schwarz, G. K. H. Madsen, and D. Kvasnicka, and J. Luitz, *WIEN2k, An Augmented Plane Wave + Local Orbitals Program for Calculating Crystal Properties* (Techn. Universität Wien, Austria, 2001).
[12] M. Aichhorn, L. Pourovskii, V. Vildosola, M. Ferrero, O. Parcollet, T. Miyake, A. Georges, and S. Biermann, Phys. Rev. B **80**, 085101 (2009).
[13] D. Faltermeier, J. Barz, M. Dumm, M. Dressel, N. Drichko, B. Petrov, V. Semkin, R. Vlasova, C. Mézière, and P. Batail, Phys. Rev. B **76**, 165113 (2007).
[14] M. Dumm, D. Faltermeier, N. Drichko, M. Dressel, C. Mézière, and P. Batail, Phys. Rev. B **79**, 195106 (2009).
[15] C. Weber, D. D. O'Regan, N. D. M. Hine, P. B. Littlewood, G. Kotliar, and M. C. Payne, Phys. Rev. Lett. **110**, 106402 (2013).
[16] W. Ku, H. Rosner, W. E. Pickett, and R. T. Scalettar, Phys. Rev. Lett. **89**, 167204 (2002).
[17] V. I. Anisimov, D. E. Kondakov, A. V. Kozhevnikov, I. A. Nekrasov, Z. V. Pchelkina, J. W. Allen, S.-K. Mo, H. D. Kim, P. Metcalf, S. Suga, A. Sekiyama, G. Keller, I. Leonov, X. Ren, and D. Vollhardt, Phys. Rev. B **71**, 125119 (2005).
[18] J. M. Williams, A. M. Kini, H. H. Wang, K. D. Carlson, U. Geiser, L. K. Montgomery, G. J. Pyrka, D. M. Watkins, J. M. Kommers, S. J. Boryscuk, A. V. S. Crouch, W. K. Kowk, J. E. Schirber, D. L. Overmyer, D. Jung, and M.-H. Whangbo, Inorg. Chem. **29**, 3272 (1990).
[19] P. Werner, A. Comanac, L. de' Medici, M. Troyer, and A. J. Millis, Phys. Rev. Lett. **97**, 076405 (2006).
[20] B. Bauer, L. D. Carr, H. G. Evertz, A. Feiguin, J. Freire, S. Fuchs, L. Gamper, J. Gukelberger, E. Gull, S. Guertler, A. Hehn, R. Igarashi, S. V. Isakov, D. Koop, P. N. Ma, P. Mates, H. Matsuo, O. Parcollet, G. Pawlowski, J. D. Picon, L. Pollet, E. Santos, V. W. Scarola, U. Schollwöck, C. Silva, B. Surer, S. Todo, S. Trebst, M. Troyer, M. L. Wall, P. Werner, and S. Wessel, J. Stat. Mech. (2011) P05001.
[21] E. Gull, P. Werner, S. Fuchs, B. Surer, T. Pruschke, and M. Troyer, Comp. Phys. Commun. **182**, 1078 (2011).
[22] K. S. D. Beach, arXiv:cond-mat/0403055.
[23] Note that in the crystallographic unit cell, there is a manifold of four bands around E_F as the crystallographic unit cell contains two organic layers with a total of four dimers due to the presence of the anion. The dimers are equivalent, though, so that only one dimer HOMO has to be considered in our single-site DMFT; the other three orbitals are related by symmetry.
[24] P. Sahebsara and D. Sénéchal, Phys. Rev. Lett. **100**, 136402 (2008).
[25] H. Lee, K. Foyevtsova, J. Ferber, M. Aichhorn, H. O. Jeschke, and R. Valentí, Phys. Rev. B **85**, 165103 (2012).
[26] K. Miyagawa, A. Kawamoto, Y. Nakazawa, and K. Kanoda, Phys. Rev. Lett. **75**, 1174 (1995).
[27] K. Kanoda, Physica C **282–287**, 299 (1997).
[28] A. M. Kini, U. Geiser, H. H. Wang, K. D. Carlson, J. M. Williams, W. K. Kwok, K. G. Vandervoort, J. E. Thompson, and D. L. A. Stupka, Inorg. Chem. **29**, 2555 (1990).
[29] X. Deng, J. Mravlje, R. Zitko, M. Ferrero, G. Kotliar, and A. Georges, Phys. Rev. Lett. **110**, 086401 (2013).